

TRAINING DEEP NORMALIZATION-FREE SPIKING NEURAL NETWORKS WITH LATERAL INHIBITION

Peiyu Liu

School of Electronics Engineering and Computer Science
Peking University
lpy512120@stu.pku.edu.cn

Jianhao Ding

School of Computer Science
Peking University

Zhaofei Yu

School of Computer Science
Peking University

ABSTRACT

Spiking neural networks (SNNs) have garnered significant attention as a central paradigm in neuromorphic computing, owing to their energy efficiency and biological plausibility. However, training deep SNNs has critically depended on explicit normalization schemes, such as batch normalization, leading to a trade-off between performance and biological realism. To resolve this conflict, we propose a normalization-free learning framework that incorporates lateral inhibition inspired by cortical circuits. Our framework replaces the traditional feedforward SNN layer with a circuit of distinct excitatory (E) and inhibitory (I) neurons that complies with Dale’s law. The circuit dynamically regulates neuronal activity through subtractive and divisive inhibition, which respectively control the activity and the gain of excitatory neurons. To enable and stabilize end-to-end training of the biologically constrained SNN, we propose two key techniques: E-I Init and E-I Prop. E-I Init is a dynamic parameter initialization scheme that balances excitatory and inhibitory inputs while performing gain control. E-I Prop decouples the backpropagation of the E-I circuits from the forward propagation and regulates gradient flow. Experiments across several datasets and network architectures demonstrate that our framework enables stable training of deep SNNs with biological realism and achieves competitive performance without resorting to explicit normalizations. Therefore, our work not only provides a solution to training deep SNNs but also serves a computational platform for further exploring the functions of lateral inhibition in large-scale cortical computation.

1 INTRODUCTION

Inspired by computational principles of biological neurons, spiking neural networks (SNNs) stand at the intersection of artificial intelligence and neuroscience (Maass, 1997; Ghosh-Dastidar & Adeli, 2009). They not only enable highly energy-efficient computation on neuromorphic hardware (Roy et al., 2019; Xiao et al., 2025) but also provide models for understanding the cortical computation across multiple scales (Kumarasinghe et al., 2021; Korcsak-Gorzo et al., 2022; N’dri et al., 2024). This duality places SNNs at the heart of the emerging field of NeuroAI (Sadeh & Clopath, 2025), fostering a synergy between artificial intelligence and neuroscience. On the one hand, a deeper understanding of brain’s computational principles offers direct inspirations for new learning algorithms and architectures in SNNs (Fang et al., 2021b; Pan et al., 2025). On the other hand, deep learning techniques have made it possible to obtain large-scale SNNs with high performance (Wu et al., 2018; Fang et al., 2021a; Bu et al., 2022). Some of these well-trained models, in turn, can serve as *in silico* platforms for investigating multi-scale cortical computations that are difficult to access through wet-lab experiments (Bellec et al., 2018).

Despite the promising synergy, realizing the potential of SNNs as an ideal platform for exploring both machine and biological intelligence is hindered by a trade-off between computational perfor-

mance and biological plausibility. Many SNN learning algorithms achieve high performance by adopting backpropagation-based techniques, treating spiking neurons as recurrent units unrolled over time (Neftci et al., 2019; Fang et al., 2021a). While this strategy yields models whose performance are comparable to their ANN counterparts, it reduces SNNs to mere deep learning artifacts, sacrificing basic biological properties. As a result, these models often ignore fundamental principles in neuroscience like the excitation-inhibition (E-I) dynamics, which are crucial in gain control (Goldwyn et al., 2018; Del Rosario et al., 2025), neural oscillation (Buzsáki & Draguhn, 2004), selective attention (Zhang et al., 2014), and so on. Consequently, deriving meaningful insights for neuroscience from these biologically unfaithful models becomes a challenge.

However, approaches that prioritize biological realism also face the challenges of unstable training. Biologically plausible learning rules such as spike-timing-dependent plasticity (STDP) (Gerstner et al., 1996; Bi & Poo, 1998), often struggle with the instability during training and thus can only be applied to shallow SNNs (Habenschuss et al., 2012; Beyeler et al., 2013). In the field of deep learning, this training instability issue is partly overcome by explicit normalization schemes, most notably batch normalization (BN) (Ioffe & Szegedy, 2015). However, while BN is a powerful tool, it depends on global statistics across mini-batches and has no known biological analogue, making it implausible for brain-inspired models. This widens the gap between high performance and biological plausibility, highlighting the need for a computationally effective and biologically grounded alternative.

Here, we address the challenge of training deep biologically plausible SNNs by introducing lateral inhibition. We propose a normalization-free learning framework for deep SNNs, based on an excitatory-inhibitory (E-I) circuit, as shown in Figure 1. Our framework presents a viable, brain-inspired alternative to standard normalization schemes, bridging the gap between high-performance deep learning and biologically plausible neural computation. The main contributions of our work can be summarized as follows:

1. We propose incorporating E-I circuits, composed of distinct excitatory and inhibitory neuron populations, into deep SNNs to enable normalization-free training.
2. To enable the training of this biologically-constrained SNN, we introduce a dynamic initialization scheme to ensure effective learning from the very beginning of training.
3. We construct a framework for stable training by integrating our initialization scheme with adaptive stabilization of divisive inhibition and a straight-through estimator (STE) method. These techniques have proven to be essential for stable learning of deep SNNs with E-I circuits.
4. We empirically validate our framework across various deep architectures. Experiments demonstrate that our biologically constrained learning framework can achieve competitive performance, indicating the viability of our brain-inspired learning algorithm.

2 RELATED WORK

2.1 NORMALIZATION METHODS IN SPIKING NEURAL NETWORKS

Recent methods for training deep SNNs can be broadly categorized into two approaches, ANN-to-SNN conversion (ANN2SNN) (Rueckauer et al., 2017; Sengupta et al., 2019; Han et al., 2020; Han & Roy, 2020; Ding et al., 2021; Stöckl & Maass, 2021; Bu et al., 2022) and direct end-to-end training through backpropagation (Lee et al., 2016; Neftci et al., 2019; Li et al., 2021; Fang et al., 2021a;b; Guo et al., 2022b; Xiao et al., 2022; Zhu et al., 2024). Normalization is critical in both ANN2SNN and training from scratch. Many ANN2SNN methods merge parameters of normalization layers in ANNs into synaptic weights of spiking neurons (Sengupta et al., 2019; Han et al., 2020; Bu et al., 2022). In contrast, training SNNs from scratch usually directly adopt normalization schemes developed for ANNs, especially BN (Ioffe & Szegedy, 2015). There are also BN-derived normalization schemes designed for SNNs, like BNTT (Kim & Panda, 2021), tdbN (Zheng et al., 2021), and TEBN (Duan et al., 2022). However, these strategies still inherit the biological implausibility of BN due to the dependence on statistics data collected from batches of inputs. Therefore, they do not fully resolve the core conflict between computational performance and biological realism, motivating the search for brain-inspired normalization alternatives.

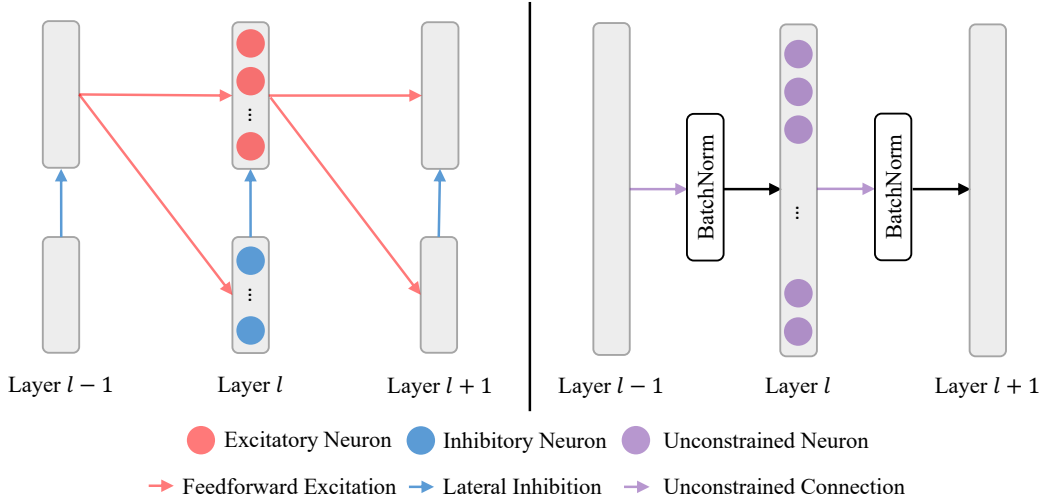


Figure 1: The proposed feedforward E-I circuit (left), compared with BN-equipped architecture (right). Neurons in layer $l - 1$ and $l + 1$ are not shown. In the E-I circuit, excitatory and inhibitory neurons are explicitly separated. In contrast, the BN architecture applies normalization operations between layers without distinguishing neuron types.

2.2 NEURAL NETWORKS WITH SEPERATE EXCITATORY AND INHIBITORY UNITS

The interplay between excitatory and inhibitory neurons has been a key topic in neuroscience (Haider et al., 2006; Ahmadian & Miller, 2021; Cohen Kadosh, 2025). Historically, computational models of these circuits has been confined to shallow networks, often focusing on the dynamics of a few interacting populations/neurons to explain foundational principles (Somers et al., 1995; Wilson & Cowan, 1972; Carandini & Heeger, 2012). One of the reasons for this limitation is that training deep networks with E-I circuits proves to be a significant challenge. This has left the whole picture of E-I dynamics largely unexplored. A remarkable step towards deep E-I networks was taken by Cornford et al. (2021). By developing techniques for parameter initialization, they demonstrated that ANNs with separate excitatory and inhibitory neuron populations could be effectively trained. However, the model is built fully with the rectified linear units (ReLU) and thus does not capture the temporal properties of the circuit. SNNs can address temporal processing, as their dynamics naturally capture temporal information. However, these initialization techniques cannot be directly applied to SNNs with E-I circuits, since the spiking dynamics introduce different constraints to SNNs compared to rate-based ReLU models.

3 PRELIMINARY

3.1 DALE’S LAW

Dale’s law is one of the most foundational principles in neuroscience, positing that most neurons exert a uniform influence on all of its postsynaptic targets, being either excitatory or inhibitory (Barranca et al., 2022). This is because a neuron releases a single type of neurotransmitter across all of its synaptic terminals, which in turn produces either an excitatory or inhibitory effect on postsynaptic neurons. When translating this principle to artificial neural networks, all outgoing synaptic weights from a given neuron should share the same sign. This makes standard initialization techniques like Xavier (Glorot & Bengio, 2010) and Kaiming (He et al., 2015) initialization inapplicable, as they sample weights from zero-centered distributions that assign both positive and negative outgoing synapse weights to each neuron.

3.2 NEURON MODEL

Excitatory neuron. We model excitatory neurons using the widely adopted leaky-integrate-and-fire (LIF) model (Gerstner et al., 2014). For a given layer l with $n_E^{[l]}$ excitatory neurons (we use superscript $[l]$ to denote the l -th layer), the sub-threshold dynamics of the membrane potential $\mathbf{u}_E^{[l]}(t) \in \mathbb{R}^{n_E^{[l]}}$ are described by the following equation:

$$\tau_E \frac{d\mathbf{u}_E^{[l]}(t)}{dt} = - \left(\mathbf{u}_E^{[l]}(t) - u_{E,\text{rest}} \right) + \mathbf{I}_E^{[l]}(t), \quad (1)$$

where τ_E and $u_{E,\text{rest}}$ are the membrane time constant and resting potential of all excitatory neurons, respectively. $\mathbf{I}_E^{[l]}(t) \in \mathbb{R}^{n_E^{[l]}}$ is the input currents to the excitatory neurons at t . For discrete-time simulation, we approximate Equation 1 using the first-order Euler method with a time step $\Delta t = 1$. By setting the resting potential $u_{E,\text{rest}}$ to 0, we obtain the following iterative update rule as follows:

$$\mathbf{u}_E^{[l]}[t+1] = \left(1 - \frac{1}{\tau_E} \right) \mathbf{u}_E^{[l]}[t] + \mathbf{I}_E^{[l]}[t], \quad (2)$$

An excitatory neuron emits a spike when its membrane potential exceeds a firing threshold θ_E (set to 1 for all excitatory neurons). To model the subsequent reset, we employ a soft reset mechanism where the potential of a firing neuron is reduced by θ_E . This leads to complete dynamics for excitatory neurons in layer l as follows:

$$\mathbf{u}_E^{[l]}[t+1] = \left(1 - \frac{1}{\tau_E} \right) \left(\mathbf{u}_E^{[l]}[t] - \theta_E \cdot \mathbf{s}_E^{[l]}[t] \right) + \mathbf{I}_E^{[l]}[t], \quad (3)$$

where the spikes are generated by Heaviside step function H , i.e., $\mathbf{s}_E^{[l]}[t] = H \left(\mathbf{u}_E^{[l]}[t] - \theta_E \right)$.

To distinguish this process from the dynamics of inhibitory neurons in layer l , we encapsulate it into an operator $\mathcal{F}_E^{[l]}$. This operator takes the input currents at the current time step as its arguments and produces the corresponding output spikes. The mapping is formally expressed as follows:

$$\mathbf{s}_E^{[l]}[t] = \mathcal{F}_E^{[l]} \left(\mathbf{I}_E^{[l]}[t]; \mathbf{u}_E^{[l]}[t], \tau_E, \theta_E \right). \quad (4)$$

Inhibitory neuron. Many inhibitory neurons, such as parvalbumin (PV)⁺ neurons, are known to be fast-spiking (FS), characterized by a much smaller membrane time constant τ_I compared to that of excitatory pyramidal neurons (Hu et al., 2014; Prince et al., 2021). In our discrete-time simulation, the time step $\Delta t = 1$ is chosen to be on a similar scale as the time constant of excitatory neurons (e.g., $\tau_E = 2$), which implies $\tau_I \ll \Delta t$. Under this condition, the dynamics of inhibitory neurons can reach a steady state almost instantaneously within a single time step. This allows us to apply an approximation to LIF model by treating τ_I as negligible, which leads to

$$0 = - \left(\mathbf{u}_I^{[l]}[t] - u_{I,\text{rest}} \right) + \mathbf{I}_I^{[l]}[t]. \quad (5)$$

Here we use notation similar to that in the excitatory neuron model, where the subscript ‘I’ denotes inhibitory neurons. By setting the resting potential $u_{I,\text{rest}}$ to 0, we find the instantaneous membrane potential is determined by its input currents:

$$\mathbf{u}_I^{[l]}[t] = \mathbf{I}_I^{[l]}[t]. \quad (6)$$

Since this potential remains constant throughout the duration of Δt , the neurons can fire $\left\lfloor \max \left(0, \mathbf{I}_I^{[l]}[t] \right) / \theta_I \right\rfloor$ times if we apply soft reset and a fixed firing threshold θ_I . Finally, by setting $\theta_I = 1$, we can directly model the total spike outputs of inhibitory neurons at time t as

$$\mathbf{s}_I^{[l]}[t] = \left\lfloor \max \left(0, \mathbf{I}_I^{[l]}[t] \right) \right\rfloor \approx \max \left(0, \mathbf{I}_I^{[l]}[t] \right). \quad (7)$$

Similar to the excitatory neuron model, we encapsulate this process into an operator $\mathcal{F}_I^{[l]}$:

$$\mathbf{s}_I^{[l]}[t] = \mathcal{F}_I^{[l]} \left(\mathbf{I}_I^{[l]}[t] \right) \approx \max \left(0, \mathbf{I}_I^{[l]}[t] \right). \quad (8)$$

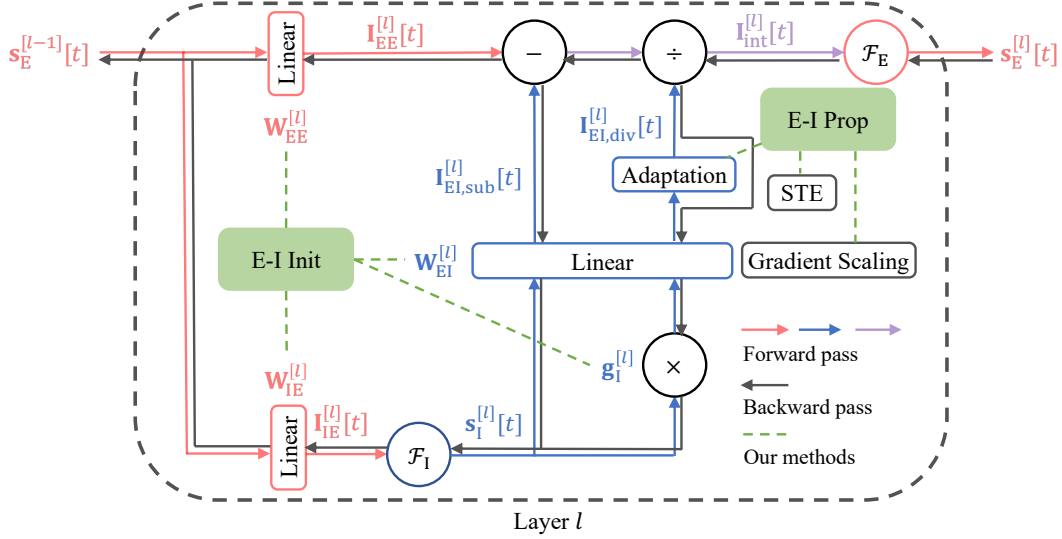


Figure 2: An overview of the proposed methods. E-I Init enables effective learning from the very beginning through a dynamic parameter initialization scheme. E-I Prop then ensures stable end-to-end training by regulating the forward and backward passes.

4 METHODS

4.1 E-I CIRCUITS IN SNNs

Our model is a feedforward SNN constructed from the canonical E-I circuit shown in Figure 1. Each layer l comprises of $n_E^{[l]}$ excitatory neurons and $n_I^{[l]}$ inhibitory neurons, where $n_E^{[l]}/n_I^{[l]} = 4$ for each layer l according to biological evidence (Markram et al., 2004). The information flow through this circuit at each time step t proceeds as follows.

Excitatory projections. First, excitatory population in layer $l - 1$ undergoes dynamics described by Equation 1 to Equation 4 and emits spikes $\mathbf{s}_E^{[l-1]}[t] \in \{0, 1\}^d$, where d is the dimension of input spikes. These input spikes project forward, simultaneously inducing two excitatory currents in both the excitatory and inhibitory populations of layer l :

$$\mathbf{I}_{EE}^{[l]}[t] = \mathbf{W}_{EE}^{[l]} \mathbf{s}_E^{[l-1]}[t], \quad (9)$$

$$\mathbf{I}_{IE}^{[l]}[t] = \mathbf{W}_{IE}^{[l]} \mathbf{s}_E^{[l-1]}[t]. \quad (10)$$

Here, subscript AB denotes a projection from population B to population A. $\mathbf{W}_{EE}^{[l]} \in \mathbb{R}^{n_E^{[l]} \times d}$ and $\mathbf{W}_{IE}^{[l]} \in \mathbb{R}^{n_I^{[l]} \times d}$ are corresponding synaptic weight matrices, which are constrained to be non-negative according to Dale’s law.

Lateral inhibition. Following the fast-spiking approximation in Section 3.2, the activity of inhibitory neurons is modeled by $\mathcal{F}_I^{[l]}$ as follows:

$$\mathbf{s}_I^{[l]}[t] = \mathcal{F}_I^{[l]} \left(\mathbf{I}_{IE}^{[l]}[t] \right). \quad (11)$$

This inhibitory signal then laterally regulates the excitatory population. Inspired by the roles of inhibition in cortex, we decompose this regulation into subtractive inhibition for E-I balance and divisive inhibition for gain control.

$$\mathbf{I}_{EI,sub}^{[l]}[t] = \mathbf{W}_{EI}^{[l]} \mathbf{s}_I^{[l]}[t], \quad (12)$$

$$\mathbf{I}_{EI,div}^{[l]}[t] = \mathbf{W}_{EI}^{[l]} \left(\mathbf{g}_I^{[l]} \odot \mathbf{s}_I^{[l]}[t] \right), \quad (13)$$

where $\mathbf{W}_{\text{EI}}^{[l]}$ is the weight matrix for inhibitory-to-excitatory projections, $\mathbf{g}_I^{[l]}$ is a trainable parameter modulating the strength of divisive inhibition, and \odot is the Hadamard product.

Input integration and spiking. Finally, the excitatory population integrates the excitatory currents with both forms of inhibition to compute the total input current.

$$\mathbf{I}_{\text{int}}^{[l]}[t] = \mathbf{g}_E^{[l]} \odot \frac{\mathbf{I}_{\text{EE}}^{[l]}[t] - \mathbf{I}_{\text{EI,sub}}^{[l]}[t]}{\mathbf{I}_{\text{EI,div}}^{[l]}[t]} + \mathbf{b}_E^{[l]}, \quad (14)$$

where $\mathbf{g}_E^{[l]}, \mathbf{b}_E^{[l]} \in \mathbb{R}^{n_E^{[l]}}$ are trainable affine transformation parameters. Using this integrated current as input current, excitatory neurons emit spikes to the next layer,

$$\mathbf{s}_E^{[l]} = \mathcal{F}_E^{[l]} \left(\mathbf{I}_{\text{int}}^{[l]}[t]; \mathbf{u}_E^{[l]}[t], \tau_E, \theta_E \right). \quad (15)$$

4.2 E-I INIT: DYNAMIC PARAMETER INITIALIZATION

Standard initialization schemes, such as Xavier (Glorot & Bengio, 2010) and Kaiming (He et al., 2015) initialization, are incompatible with E-I circuits since their assumption of zero-centered weight distributions directly violates Dale’s law, which imposes strict sign constraints on synaptic weights. A naive initialization under this constraint can easily lead to pathological network activity, making the training of deep architectures infeasible (see Section 5.2). Therefore, we propose E-I Init, an initialization scheme designed for deep SNNs with E-I circuits. Its design is guided by two primary objectives: establishing an initial E-I balance to ensure neurons operate in a responsive state, preventing them from silencing or saturating, and setting an initial activity for gain control to ensure stable signal propagation from the start of training.

E-I balance by subtractive inhibition. A key goal of our initialization scheme is to ensure that neurons operate in a responsive regime. We achieve this by setting the expected subtractive inhibitory current to approximately balance the expected excitatory current, which is defined as

$$\mathbb{E} \left[\mathbf{I}_{\text{EE},i}^{[l]} \right] \approx \mathbb{E} \left[\mathbf{I}_{\text{EI,sub},i}^{[l]} \right], \quad (16)$$

for each neuron i in layer l and results in a near-zero expected net input, preventing neurons from being saturated or silent at initialization. To implement this under the constraint of Dale’s law, we draw inspiration from Cornford et al. (2021) and leverage the exponential distribution for weight initialization. Specifically, we draw the excitatory weights $\mathbf{W}_{\text{EE}}^{[l]}$ and $\mathbf{W}_{\text{IE}}^{[l]}$ from an exponential distribution with a shared rate parameter $\lambda^{[l]}$. The inhibitory weights $\mathbf{W}_{\text{EI}}^{[l]}$ are deterministically set to $1/n_I^{[l]}$ to uniformly distribute the inhibitory signals. Assuming that presynaptic neurons fire independently with an average probability of p (i.e., the spike from each neuron at any time step is an identical and independent Bernoulli trial with probability p), the expected excitatory input to neuron i in layer l is

$$\mathbb{E} \left[\mathbf{I}_{\text{EE},i}^{[l]} \right] = dp \mathbb{E} \left[\mathbf{W}_{\text{EE}}^{[l]} \right], \quad (17)$$

where d is the dimension of input spikes. Similarly, the expected subtractive inhibitory current is

$$\mathbb{E} \left[\mathbf{I}_{\text{EI,sub},i}^{[l]} \right] = n_I^{[l]} dp \mathbb{E} \left[\mathbf{W}_{\text{IE}}^{[l]} \right] \mathbb{E} \left[\mathbf{W}_{\text{EI}}^{[l]} \right]. \quad (18)$$

Therefore, by setting $\mathbb{E} \left[\mathbf{W}_{\text{EE}}^{[l]} \right] = \mathbb{E} \left[\mathbf{W}_{\text{IE}}^{[l]} \right] = 1/\lambda^{[l]}$ and $\mathbf{W}_{\text{EI}}^{[l]} = 1/n_I^{[l]}$, we arrive at the desired balance defined by Equation 16.

Gain control by divisive inhibition. Our second objective to establish stable signal propagation by setting an appropriate initial gain for excitatory neurons. In our model, gain is primarily modulated by the divisive inhibitory current. Inspired by normalization techniques, our strategy is to modulate divisive inhibition through $\mathbf{g}_I^{[l]}$ such that the expected value of this divisive inhibitory current approximates the standard deviation of the excitatory inputs for each neuron i . This can be formulated as

$$\mathbb{E} \left[\mathbf{I}_{\text{EI,div},i}^{[l]} \right] = \text{std} \left(\mathbf{I}_{\text{EE},i}^{[l]} \right) \quad (19)$$

for each neuron i in layer l . In this way, the divisive operation effectively scales the final input, leading the excitatory neurons to a responsive regime at initialization. Similar to Equation 18, for inhibitory neuron i in layer l ,

$$\mathbb{E} \left[\mathbf{I}_{\text{EI,div},i}^{[l]} \right] = n_i^{[l]} dp \mathbb{E} \left[\mathbf{g}_i^{[l]} \right] \mathbb{E} \left[\mathbf{W}_{\text{IE}}^{[l]} \right] \mathbb{E} \left[\mathbf{W}_{\text{EI}}^{[l]} \right] = \frac{dp \mathbb{E} \left[\mathbf{g}_i^{[l]} \right]}{\lambda^{[l]}}. \quad (20)$$

By assuming spike from each neuron at any time step is an identical and independent Bernoulli trial with probability p , the standard deviation of excitatory input current of neuron i can be formulated as

$$\text{std} \left(\mathbf{I}_{\text{EE},i}^{[l]} \right) = \frac{\sqrt{dp(2-p)}}{\lambda^{[l]}}, \quad (21)$$

see Appendix A.4.1 for details. Therefore, by setting each element of $\mathbf{g}_i^{[l]}$ to $\sqrt{\frac{2-p}{dp}}$, we obtain a normalization effect at initialization, making the effective training of deep SNNs possible.

Initialization of other parameters. Finally, we initialize $\lambda^{[l]} = \sqrt{\frac{d(2-p)}{1-p}}$ to meet the condition $\text{std} \left(\mathbf{I}_{\text{EE},i}^{[l]} \right) = \sqrt{p(1-p)}$ (see Appendix A.4.2). $\mathbf{g}_E^{[l]}$ and $\mathbf{b}_E^{[l]}$ are initialized as vector $\mathbf{1}$ and $\mathbf{0}$, respectively.

Dynamic firing probability estimation. Since the initialization depends on averaged firing probability p , we use the first batch in training set to compute point estimations of p and other statistics, leading to a dynamic initialization regime.

4.3 E-I PROP: STABILIZING END-TO-END TRAINING

While E-I Init provides a stable initial state, the interplay between divisive inhibition and discrete spikes causes training instabilities. These arise mainly from two sources: first, near-zero divisive terms in the forward pass that trigger numerical explosions; and second, disproportionately large gradients in the lateral inhibitory pathway during backpropagation, which destabilize learning. To overcome this, we propose E-I Prop, a method that decouples the backpropagation of E-I circuits from forward propagation and regulates gradient flow. Forward stability is ensured by adaptive divisive inhibition, while backward stability is achieved through a straight-through estimator (STE) combined with gradient scaling.

Adaptive stabilization of divisive inhibition. To prevent division-by-zero errors in the forward pass, a common technique is to add a small constant ϵ to the denominator. However, a fixed ϵ is ill-suited for our network because the divisive inhibitory current is designed to provide a suitable dynamic range of final integrated currents and thus to perform gain control. A pre-defined ϵ that is too small may fail to prevent numerical instability if the denominator collapses towards zero, while one that is too large will artificially suppress the dynamic range by dominating the denominator, thus undermining the purpose of gain control. To overcome this limitation, we propose an adaptive stabilization method. Instead of using a static constant, our approach sets a dynamic, input-dependent lower bound for the denominator. Specifically, for each sample within a batch, we identify any zero values in $\mathbf{I}_{\text{EI,div}}$. Then these zero values are replaced by the smallest positive value found within the same sample, which proves to be necessary for effective training (see Section 5.2 for details).

Straight-through estimator. A main drawback with our adaptive stabilization mechanism is that the replacement operation (i.e., substituting zeros with the smallest positive value) is non-differentiable. This means that the gradient cannot flow back to the network parameters that caused the denominator to become zero during forward pass. Instead, the gradient path is incorrectly rerouted to the positions that produced the smallest positive value. This misdirected gradient flow can destabilize the learning process. To overcome this, we employ the straight-through estimator (STE), a common technique for handling non-differentiable operations in neural networks (Liu & Mattina, 2019). In the forward pass, we perform the adaptive stabilization as described, replacing any zeros to ensure numerical stability and proper gain control. In the backward pass, we approximate the derivative of this non-differentiable operation with a simple identity function (see Appendix A.5 for detailed implementation). This approach effectively decouples the forward-pass requirement for numerical stability from the backward-pass requirement for a clean gradient path, ensuring that the network can learn robustly.

Gradient scaling. To ensure stable training, it is crucial to balance the influence of the feedforward excitatory and lateral inhibitory pathways on parameter updates. Empirical analysis shows that gradients for lateral inhibitory weight, $\mathbf{W}_{EI}^{[l]}$, are disproportionately larger than other synaptic weights (see Appendix A.6.2). This imbalance can destabilize the learning process. To resolve this, we scale the gradient of the inhibitory weight $\mathbf{W}_{EI}^{[l]}$ by a factor of $1/d$, where d is the dimension of the input spikes. This effectively balances the update magnitudes between the two pathways and thus enables stable learning.

As illustrated in Figure 2, our method provides a complete learning framework composed of E-I Init and E-I Prop, enabling stable and effective end-to-end training from scratch.

5 EXPERIMENTS

5.1 PERFORMANCE ON IMAGE CLASSIFICATION

We test our methods on CIFAR-10/100 (Krizhevsky, 2009) against other models. All results are summarized in Table 1. On the CIFAR-10 dataset, our model achieves top-1 accuracies of 92.12% on ResNet-18 (He et al., 2016; Fang et al., 2021a) with 4 time steps. This performance surpasses all other presented normalization-free and E-I constrained SNN baselines and proves the effectiveness of our learning framework in training very deep and biologically-constrained SNNs without explicit normalization. On the more challenging CIFAR-100 dataset, our model reaches 65.53% on VGG-16 (Simonyan & Zisserman, 2015), which demonstrates that our method generalizes well to more complex tasks. Collectively, these results validate that our proposed E-I circuit, empowered by the E-I Init and E-I Prop, is a scalable and effective alternative to explicit normalization.

Table 1: Comparison with biologically constrained, normalization-free and BN-equipped SNNs.

Dataset	Model	Type	E-I	Norm.	Arch.	T	Acc.(%)	
CIFAR-10	DAP (Micheli et al., 2025)	SNN	N	N	7-layer CNN	3	57.52	
	FDI (Rossbroich et al., 2022)	SNN	Y	N	6-layer CNN	50	65.60	
	SRI (Ding et al., 2025)	SNN	N	N	VGG-9	20	87.62	
	B-SNN (Karimah et al., 2025)	SNN	N	N	VGG-8	64	87.73	
	IM-Loss (Guo et al., 2022a)	SNN	N	N	CIFARNet	4	90.90	
	BackEISNN (Zhao et al., 2022)	SNN	Y	N	5-layer CNN	20	90.93	
	EICIL (Shao et al., 2023)	SNN	N	Y	N	ResNet-18	–	90.34
						E-I Net	–	89.43
	DANN Cornford et al. (2021)	ANN	Y	N	N	VGG-16	–	88.67
						VGG-19	–	88.12
	SNN with default BN	SNN	N	N	Y	VGG-16	4	94.37
						VGG-19	4	94.18
						ResNet-18	4	95.57
	DeepEISNN (Ours)	SNN	Y	N	N	VGG-16	4	90.75
VGG-19						4	91.20	
ResNet-18						4	92.12	
SRI (Ding et al., 2025)	SNN	N	N	N	VGG-11	20	54.94	
CIFAR-100	EICIL (Shao et al., 2023)	SNN	N	N	ResNet-18	–	63.47	
					E-I Net	–	53.86	
DeepEISNN (Ours)	SNN	Y	N	N	VGG-16	4	65.53	
					VGG-19	4	65.11	

5.2 ABLATION STUDY

Results of ablation study are summarized in Table 2. It confirms that each component in our method is indispensable for stable and high-performance training. Replacing E-I Init with a standard Kaiming initialization leads to either a complete training failure or a significant accuracy drop, proving

its necessity for establishing a proper E-I balance and gain control. Furthermore, the common ϵ -stabilization fails across all tested values, confirming that our adaptive stabilization mechanism is crucial for maintaining both numerical stability and gain control. Finally, removing gradient scaling from inhibitory synapses causes training collapse, which validates its role in balancing learning dynamics. These findings demonstrate that E-I Init, adaptive stabilization of divisive inhibition, and gradient scaling are necessary mechanisms for effective training.

Table 2: Results of ablation study with VGG-8 on CIFAR-10.

Method	Configuration	Acc.(%)
DeepEISNN (Ours)	Full methods	87.03
Clamped Kaiming normal initialization	Kaiming init. on W_{EE} & W_{IE} Kaiming init. on W_{EE} , W_{IE} & W_{EI}	85.61 Fails to train
ϵ -stabilization	$\epsilon = 10^{-8}$	Fails to train
	$\epsilon = 10^{-7}$	Fails to train
	$\epsilon = 10^{-6}$	Collapses (Epoch 22)
	$\epsilon = 10^{-5}$	Collapses (Epoch 5)
w/o gradient scaling	No gradient scaling on W_{EI}	Collapses (Epoch 10)

5.3 DISTRIBUTION OF INTEGRATED CURRENTS

Visualization of the integrated current distributions reveals that our framework leverages a normalization-like effect at initialization but ultimately learns a more sophisticated, dynamic mechanism. As shown in Figure 3, E-I Init successfully produces stable, zero-centered distributions, providing a crucial normalized starting point for training. However, after training, some of the distributions evolve into a distinct bimodal shape, in contrast to the Gaussian output of a SNN with default BN (see Appendix A.6.4). This emergent bimodality demonstrates that the E-I circuit’s final strategy is not simple normalization, but a dynamic separation of neurons into activated and suppressed populations, confirming its role as a powerful, learned alternative to normalization.

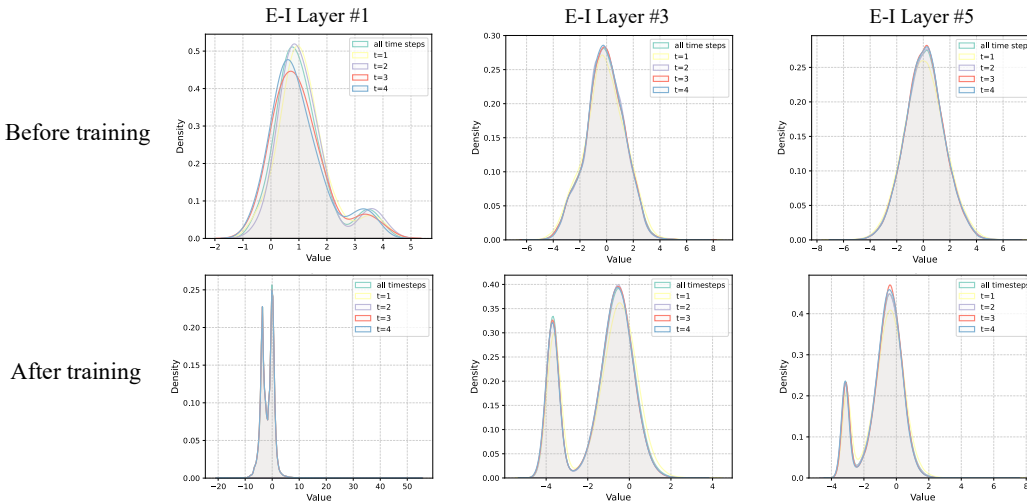


Figure 3: Distributions of the integrated input currents in the 1st, 3rd and 5th layers of our model before and after training.

6 CONCLUSION AND DISCUSSION

In this work, we address the critical challenge of training deep, biologically plausible SNNs without explicit normalization by introducing lateral inhibition. Through a principled initialization scheme, E-I Init, and a suite of stabilization techniques, E-I Prop, we enable the stable end-to-end training of deep E-I SNNs that adhere to Dale’s law. Our experiments demonstrate that this framework not only achieves competitive performance on several benchmarks but also learns a sophisticated form of activity regulation that is functionally distinct from standard normalization. We show that the E-I circuit uses an initial normalization-like state as a scaffold to ultimately learn a sparse representation. Therefore, our work provides both a practical solution for building powerful, normalization-free SNNs and a compelling computational model for exploring how canonical cortical circuits perform complex computations, further bridging the gap between deep learning and neuroscience.

REFERENCES

- Yashar Ahmadian and Kenneth D. Miller. What is the dynamical regime of cerebral cortex? *Neuron*, 109(21):3373–3391, 2021.
- Victor J. Barranca, Asha Bhuiyan, Max Sundgren, and Fangzhou Xing. Functional implications of Dale’s law in balanced neuronal network dynamics and decision making. *Frontiers in Neuroscience*, 16:801847, 2022.
- Guillaume Bellec, Darjan Salaj, Anand Subramoney, Robert Legenstein, and Wolfgang Maass. Long short-term memory and learning-to-learn in networks of spiking neurons. In *Advances in Neural Information Processing Systems*, pp. 795–805, 2018.
- Michael Beyeler, Nikil D. Dutt, and Jeffrey L. Krichmar. Categorization and decision-making in a neurobiologically plausible spiking network using a STDP-like learning rule. *Neural Network*, 48:109–124, 2013.
- Guo-qiang Bi and Mu-ming Poo. Synaptic modifications in cultured hippocampal neurons: dependence on spike timing, synaptic strength, and postsynaptic cell type. *Journal of Neuroscience*, 18(24):10464–10472, 1998.
- Tong Bu, Wei Fang, Jianhao Ding, PengLin Dai, Zhaofei Yu, and Tiejun Huang. Optimal ANN-SNN conversion for high-accuracy and ultra-low-latency spiking neural networks. In *International Conference on Learning Representations*, 2022.
- György Buzsáki and Andreas Draguhn. Neuronal oscillations in cortical networks. *Science*, 304:1926–1929, 2004.
- Matteo Carandini and David J. Heeger. Normalization as a canonical neural computation. *Nature Reviews Neuroscience*, 13:51–62, 2012.
- Roi Cohen Kadosh. Rethinking excitation/inhibition balance in the human brain. *Nature Reviews Neuroscience*, 26(8):451–452, 2025.
- Jonathan Cornford, Damjan Kalajdzievski, Marco Leite, Amélie Lamarquette, Dimitri Michael Kullmann, and Blake Aaron Richards. Learning to live with Dale’s principle: ANNs with separate excitatory and inhibitory units. In *International Conference on Learning Representations*, 2021.
- Joseph Del Rosario, Stefano Coletta, Soon Ho Kim, Zach Mobbille, Kayla Peelman, Brice Williams, Alan J. Otsuki, Alejandra Del Castillo Valerio, Kendell Worden, Lou T. Blanpain, Lyndah Lovell, Hannah Choi, and Bilal Haider. Lateral inhibition in v1 controls neural and perceptual contrast sensitivity. *Nature Neuroscience*, 28:836–847, 2025.
- Jianhao Ding, Zhaofei Yu, Yonghong Tian, and Tiejun Huang. Optimal ANN-SNN conversion for fast and accurate inference in deep spiking neural networks. In *International Joint Conference on Artificial Intelligence*, pp. 2328–2336, 2021.
- Jianhao Ding, Jiyan Zhang, Tiejun Huang, Jian K. Liu, and Zhaofei Yu. Assisting training of deep spiking neural networks with parameter initialization. *IEEE Transactions on Neural Networks and Learning Systems*, 36(8):15015–15028, 2025.

- Chaoteng Duan, Jianhao Ding, Shiyan Chen, Zhaofei Yu, and Tiejun Huang. Temporal effective batch normalization in spiking neural networks. In *Advances in Neural Information Processing Systems*, volume 35, pp. 34377–34390, 2022.
- Wei Fang, Zhaofei Yu, Yanqi Chen, Tiejun Huang, Timothée Masquelier, and Yonghong Tian. Deep residual learning in spiking neural networks. In *Advances in Neural Information Processing Systems*, volume 34, pp. 21056–21069, 2021a.
- Wei Fang, Zhaofei Yu, Yanqi Chen, Timothée Masquelier, Tiejun Huang, and Yonghong Tian. Incorporating learnable membrane time constant to enhance learning of spiking neural networks. In *Proceedings of the IEEE/CVF International Conference on Computer Vision*, pp. 2641–2651, 2021b.
- Wulfram Gerstner, Richard Kempter, J. Leo van Hemmen, and Hermann Wagner. A neuronal learning rule for sub-millisecond temporal coding. *Nature*, 383:76–78, 1996.
- Wulfram Gerstner, Werner M. Kistler, Richard Naud, and Liam Paninski. *Neuronal Dynamics: From Single Neurons to Networks and Models of Cognition*. Cambridge University Press, 2014.
- S. Ghosh-Dastidar and H. Adeli. Spiking neural networks. *International Journal of Neural Systems*, 19(04):295–308, 2009.
- Xavier Glorot and Yoshua Bengio. Understanding the difficulty of training deep feedforward neural networks. In *Proceedings of the Thirteenth International Conference on Artificial Intelligence and Statistics, AISTATS*, volume 9, pp. 249–256, 2010.
- Joshua H. Goldwyn, Bradley R. Slabe, Joseph B. Travers, and David Terman. Gain control with A-type potassium current: IA as a switch between divisive and subtractive inhibition. *PLOS Computational Biology*, 14:1–23, 2018.
- Yufei Guo, Yuanpei Chen, Liwen Zhang, Xiaode Liu, Yinglei Wang, Xuhui Huang, and Zhe Ma. IM-Loss: Information maximization loss for spiking neural networks. In S. Koyejo, S. Mohamed, A. Agarwal, D. Belgrave, K. Cho, and A. Oh (eds.), *Advances in Neural Information Processing Systems*, volume 35, pp. 156–166, 2022a.
- Yufei Guo, Xinyi Tong, Yuanpei Chen, Liwen Zhang, Xiaode Liu, Zhe Ma, and Xuhui Huang. RecDis-SNN: Rectifying membrane potential distribution for directly training spiking neural networks. In *Proceedings of the IEEE/CVF International Conference on Computer Vision*, pp. 326–335, 2022b.
- Stefan Habenschuss, Johannes Bill, and Bernhard Nessler. Homeostatic plasticity in Bayesian spiking networks as expectation maximization with posterior constraints. In *Advances in Neural Information Processing Systems*, volume 25, 2012.
- Bilal Haider, Alvaro Duque, Andrea R. Hasenstaub, and David A. McCormick. Neocortical network activity In Vivo is generated through a dynamic balance of excitation and inhibition. *Journal of Neuroscience*, 26(17):4535–4545, 2006.
- Bing Han and Kaushik Roy. Deep spiking neural network: Energy efficiency through time based coding. In *European Conference on Computer Vision*, pp. 388–404. Springer, 2020.
- Bing Han, Gopalakrishnan Srinivasan, and Kaushik Roy. RMP-SNN: Residual membrane potential neuron for enabling deeper high-accuracy and low-latency spiking neural network. In *Proceedings of the IEEE/CVF International Conference on Computer Vision*, pp. 13555–13564, 2020.
- Kaiming He, Xiangyu Zhang, Shaoqing Ren, and Jian Sun. Delving deep into rectifiers: Surpassing human-level performance on ImageNet classification. In *Proceedings of the IEEE/CVF International Conference on Computer Vision*, pp. 1026–1034, 2015.
- Kaiming He, Xiangyu Zhang, Shaoqing Ren, and Jian Sun. Deep residual learning for image recognition. In *Proceedings of the IEEE/CVF International Conference on Computer Vision*, pp. 770–778, 2016.

- Hua Hu, Jian Gan, and Peter Jonas. Fast-spiking, parvalbumin⁺ GABAergic interneurons: From cellular design to microcircuit function. *Science*, 345(6196):1255263, 2014.
- Sergey Ioffe and Christian Szegedy. Batch normalization: accelerating deep network training by reducing internal covariate shift. In *Proceedings of the 38th International Conference on Machine Learning*, pp. 448–456, 2015.
- Hasna Nur Karimah, Chankyu Lee, and Yeongkyo Seo. Batchnorm-free binarized deep spiking neural network for a lightweight machine learning model. *Electronics*, 14(8):1602, 2025.
- Youngeun Kim and Priyadarshini Panda. Revisiting batch normalization for training low-latency deep spiking neural networks from scratch. *Frontiers in Neuroscience*, 15:773954–773954, 2021.
- Agnes Korcsak-Gorzo, Michael G. Müller, Andreas Baumbach, Luziwei Leng, Oliver J. Breitwieser, Sacha J. van Albada, Walter Senn, Karlheinz Meier, Robert Legenstein, and Mihai A. Petrovici. Cortical oscillations support sampling-based computations in spiking neural networks. *PLOS Computational Biology*, 18:1–41, 2022.
- Alex Krizhevsky. Learning multiple layers of features from tiny images. 2009.
- Kaushalya Kumarasinghe, Nikola Kasabov, and Denise Taylor. Brain-inspired spiking neural networks for decoding and understanding muscle activity and kinematics from electroencephalography signals during hand movements. *Scientific Reports*, 11(1):2486, 2021.
- Jun Haeng Lee, Tobi Delbruck, and Michael Pfeiffer. Training deep spiking neural networks using backpropagation. *Frontiers in Neuroscience*, 10:508, 2016.
- Yuhang Li, Yufei Guo, Shanghang Zhang, Shikuang Deng, Yongqing Hai, and Shi Gu. Differentiable Spike: Rethinking gradient-descent for training spiking neural networks. In *Advances in Neural Information Processing Systems*, volume 34, pp. 23426–23439, 2021.
- Zhi-Gang Liu and Matthew Mattina. Learning low-precision neural networks without straight-through estimator (STE). In *International Joint Conference on Artificial Intelligence*, pp. 3066–3072, 2019.
- Wolfgang Maass. Networks of spiking neurons: the third generation of neural network models. *Neural Networks*, 10(9):1659–1671, 1997.
- Henry Markram, Maria Toledo-Rodriguez, Yun Wang, Anirudh Gupta, Gilad Silberberg, and Caizhi Wu. Interneurons of the neocortical inhibitory system. *Nature Reviews Neuroscience*, 5(10):793–807, 2004.
- Aurora Micheli, Olaf Booi, Jan van Gemert, and Nergis Tömen. Deep activity propagation via weight initialization in spiking neural networks. In *Neuro Inspired Computational Elements (NICE)*, pp. 1–9, 2025.
- Antony W. N’dri, William Gebhardt, Céline Teulière, Fleur Zeldenrust, Rajesh P. N. Rao, Jochen Triesch, and Alexander Ororbia. Predictive coding with spiking neural networks: a survey, 2024.
- Emre O. Neftci, Hesham Mostafa, and Friedemann Zenke. Surrogate gradient learning in spiking neural networks: bringing the power of gradient-based optimization to spiking neural networks. *IEEE Signal Processing Magazine*, 36:51–63, 2019.
- Yuqi Pan, Yupeng Feng, Jinghao Zhuang, Siyu Ding, Zehao Liu, Bohan Sun, Yuhong Chou, Han Xu, Xuerui Qiu, Anlin Deng, Anjie Hu, Peng Zhou, Man Yao, Jibin Wu, Jian Yang, Guoliang Sun, Bo Xu, and Guoqi Li. SpikingBrain technical report: spiking brain-inspired large models. *arXiv preprint arXiv:2509.05276*, 2025.
- Luke Y. Prince, Matthew M. Tran, Dorian Grey, Lydia Saad, Helen Chasiotis, Jeehyun Kwag, Michael M. Kohl, and Blake A. Richards. Neocortical inhibitory interneuron subtypes are differentially attuned to synchrony- and rate-coded information. *Communications Biology*, 4(1):935, 2021.

- Julian Rossbroich, Julia Gyga, and Friedemann Zenke. Fluctuation-driven initialization for spiking neural network training. *Neuromorphic Computing and Engineering*, 2(4):044016, 2022.
- Kaushik Roy, Akhilesh Jaiswal, and Priyadarshini Panda. Towards spike-based machine intelligence with neuromorphic computing. *Nature*, 575:607–617, 2019.
- Bodo Rueckauer, Iulia-Alexandra Lungu, Yuhuang Hu, Michael Pfeiffer, and Shih-Chii Liu. Conversion of continuous-valued deep networks to efficient event-driven networks for image classification. *Frontiers in Neuroscience*, 11:682, 2017.
- Sadra Sadeh and Claudia Clopath. The emergence of NeuroAI: bridging neuroscience and artificial intelligence. *Nature Reviews Neuroscience*, 26:583–584, 2025.
- Abhronil Sengupta, Yuting Ye, Robert Wang, Chiao Liu, and Kaushik Roy. Going deeper in spiking neural networks: VGG and residual architectures. *Frontiers in Neuroscience*, 13:95, 2019.
- Zihang Shao, Xuanye Fang, Yaxin Li, Chaoran Feng, Jiangrong Shen, and Qi Xu. EICIL: Joint excitatory inhibitory cycle iteration learning for deep spiking neural networks. In *Advances in Neural Information Processing Systems*, volume 36, pp. 32117–32128, 2023.
- Karen Simonyan and Andrew Zisserman. Very deep convolutional networks for large-scale image recognition. In *International Conference on Learning Representations*, 2015.
- DC Somers, SB Nelson, and M Sur. An emergent model of orientation selectivity in cat visual cortical simple cells. *Journal of Neuroscience*, 15(8):5448–5465, 1995.
- Christoph Stöckl and Wolfgang Maass. Optimized spiking neurons can classify images with high accuracy through temporal coding with two spikes. *Nature Machine Intelligence*, 3(3):230–238, 2021.
- Hugh R. Wilson and Jack D. Cowan. Excitatory and inhibitory interactions in localized populations of model neurons. *Biophysical Journal*, 12(1):1–24, 1972.
- Yujie Wu, Lei Deng, Guoqi Li, Jun Zhu, and Luping Shi. Spatio-temporal backpropagation for training high-performance spiking neural networks. *Frontiers in Neuroscience*, 12:331, 2018.
- Mingqing Xiao, Qingyan Meng, Zongpeng Zhang, Di He, and Zhouchen Lin. Online training through time for spiking neural networks. In *Advances in Neural Information Processing Systems*, volume 35, pp. 20717–20730, 2022.
- Yu Xiao, Yize Liu, Bihua Zhang, Peng Chen, Huaze Zhu, Enhui He, Jiayi Zhao, Wenju Huo, Xiaofei Jin, Xumeng Zhang, et al. Bio-plausible reconfigurable spiking neuron for neuromorphic computing. *Science Advances*, 11(6):eadr6733, 2025.
- Siyu Zhang, Min Xu, Tsukasa Kamigaki, Johnny Phong Hoang Do, Wei-Cheng Chang, Sean Jenvay, Kazunari Miyamichi, Liqun Luo, and Yang Dan. Long-range and local circuits for top-down modulation of visual cortex processing. *Science*, pp. 660–665, 2014.
- Dongcheng Zhao, Yi Zeng, and Yang Li. BackEISnn: A deep spiking neural network with adaptive self-feedback and balanced excitatory–inhibitory neurons. *Neural Networks*, 154:68–77, 2022.
- Hanle Zheng, Yujie Wu, Lei Deng, Yifan Hu, and Guoqi Li. Going deeper with directly-trained larger spiking neural networks. In *Proceedings of the AAAI Conference on Artificial Intelligence*, volume 35, pp. 11062–11070, 2021.
- Yaoyu Zhu, Jianhao Ding, Tiejun Huang, Xiaodong Xie, and Zhaofei Yu. Online stabilization of spiking neural networks. In *International Conference on Learning Representations*, 2024.

A APPENDIX

A.1 LLM USAGE

We utilized large language model to assist in proofreading and enhancing the clarity and readability of the manuscript. The core scientific contributions, experimental design, and data analysis are conducted entirely by the authors.

A.2 REPRODUCIBILITY STATEMENT

All essential details regarding datasets, model architectures, and training hyperparameters are provided in Section 5 and Appendix A.6.1 to ensure reproducibility. The source code for our framework will be made publicly available upon the publication of this paper.

A.3 ETHICS STATEMENT

This work is foundational research focused on algorithms for brain-inspired neural networks and exclusively uses standard public datasets (CIFAR-10/100). We do not foresee any direct negative societal impacts or ethical concerns arising from this research.

A.4 SUPPLEMENTAL DERIVATIONS FOR E-I INIT

This section provides detailed derivations for the expressions introduced in the E-I Init method (Section 4.2), using the same notation as the main text.

A.4.1 DERIVATION OF THE STANDARD DEVIATION OF EXCITATORY INPUT CURRENT

According to the definition of a linear transformation, the variance of the excitatory input current to neuron i is:

$$\text{Var} \left(\mathbf{I}_{\text{EE},i}^{[l]} \right) = \text{Var} \left(\sum_{j=1}^d \mathbf{W}_{\text{EE},ij}^{[l]} s_{\text{E},j}^{[l-1]} \right), \quad (22)$$

where $\mathbf{W}_{\text{EE},ij}$ denotes the element at (i, j) of the weight matrix $\mathbf{W}_{\text{EE}}^{[l]}$. Assuming the terms $\mathbf{W}_{\text{EE},ij}^{[l]} s_{\text{E},j}^{[l-1]}$ are independent for each j , the variance of the sum is the sum of the variances:

$$\text{Var} \left(\mathbf{I}_{\text{EE},i}^{[l]} \right) = \sum_{j=1}^d \text{Var} \left(\mathbf{W}_{\text{EE},ij}^{[l]} s_{\text{E},j}^{[l-1]} \right). \quad (23)$$

By further assuming that the weights $\mathbf{W}_{\text{EE},ij}$ and input spikes $s_{\text{E},j}^{[l-1]}$ are independent distributed, we can simplify this to

$$\text{Var} \left(\mathbf{I}_{\text{EE},i}^{[l]} \right) = d \cdot \text{Var} \left(\mathbf{W}_{\text{EE}}^{[l]} s_{\text{E}}^{[l-1]} \right) \quad (24)$$

$$= d \left(\mathbb{E} \left[(s_{\text{E}}^{[l-1]})^2 \right] \text{Var} \left(\mathbf{W}_{\text{EE}}^{[l]} \right) + \text{Var} \left(s_{\text{E}}^{[l-1]} \right) \mathbb{E}^2 \left[\mathbf{W}_{\text{EE}}^{[l]} \right] \right). \quad (25)$$

As established in the main text, we model the input spikes as following a Bernoulli distribution with parameter p . Thus, $\mathbb{E} \left[s_{\text{E}}^{[l-1]} \right] = p$, $\mathbb{E} \left[(s_{\text{E}}^{[l-1]})^2 \right] = p$, and $\text{Var} \left(s_{\text{E}}^{[l-1]} \right) = p(1-p)$. The weights $\mathbf{W}_{\text{EE}}^{[l]}$ are drawn from an exponential distribution with rate $\lambda^{[l]}$, for which $\mathbb{E} \left[\mathbf{W}_{\text{EE}}^{[l]} \right] = 1/\lambda^{[l]}$ and $\text{Var} \left(\mathbf{W}_{\text{EE}}^{[l]} \right) = 1/(\lambda^{[l]})^2$. Substituting these into the equation yields:

$$\text{Var} \left(\mathbf{I}_{\text{EE},i}^{[l]} \right) = d \left(p \cdot \frac{1}{(\lambda^{[l]})^2} + p(1-p) \cdot \frac{1}{(\lambda^{[l]})^2} \right) \quad (26)$$

$$= \frac{d}{(\lambda^{[l]})^2} (p + p(1-p)) \quad (27)$$

$$= \frac{dp(2-p)}{(\lambda^{[l]})^2}. \quad (28)$$

Therefore, the standard deviation of $\mathbf{I}_{EE,i}^{[l]}$ is:

$$\text{std} \left(\mathbf{I}_{EE,i}^{[l]} \right) = \sqrt{\text{Var} \left(\mathbf{I}_{EE,i}^{[l]} \right)} = \frac{\sqrt{dp(2-p)}}{\lambda^{[l]}}. \quad (29)$$

A.4.2 DERIVATION OF THE RATE PARAMETER $\lambda^{[l]}$

To ensure stable signal propagation at initialization, we set the standard deviation of the input current to match that of the input spikes, i.e., $\text{std} \left(\mathbf{I}_{EE,i}^{[l]} \right) = \text{std} \left(s_E^{[l-1]} \right) = \sqrt{p(1-p)}$. Using the result from Equation 29:

$$\frac{\sqrt{dp(2-p)}}{\lambda^{[l]}} = \sqrt{p(1-p)} \quad (30)$$

$$\lambda^{[l]} = \frac{\sqrt{dp(2-p)}}{\sqrt{p(1-p)}} = \sqrt{\frac{d(2-p)}{1-p}}. \quad (31)$$

A.5 IMPLEMENTATION OF ADAPTIVE INHIBITION WITH STE

Algorithm 1 demonstrates the full procedure of our proposed adaptive stabilization of divisive inhibition mechanism, including the custom backward pass for the STE.

Algorithm 1 Adaptive Zero Replacement with Straight-Through Estimator (STE)

Require: Input tensor tX of shape (B, \dots) , where B is the batch size.

Ensure: Output tensor \mathbf{X}_{out} with zeros adaptively replaced.

```

1: procedure ADAPTIVEZEROREPLACEMENT( $\mathbf{X}$ )
2:   if  $\mathbf{X}$  contains no zero values then
3:     return  $\mathbf{X}$ 
4:   end if
5:      $\mathbf{M} \leftarrow (\mathbf{X} == 0)$  ▷ Step 1: Determine the output value for the forward pass
6:      $\mathbf{X}_{\text{tmp}} \leftarrow \mathbf{X}$  ▷ Create a boolean mask for all zero locations.
7:      $\mathbf{X}_{\text{tmp}}[\mathbf{M}] \leftarrow \infty$  ▷ Temporarily replace zeros with infinity.
8:     Initialize an empty tensor  $\mathbf{S}$  with the same shape as a single sample in  $\mathbf{X}$ .
9:     for each sample  $i$  from 1 to  $B$  do
10:        $s_i \leftarrow \min(\mathbf{X}_{\text{tmp}}[i])$  ▷ Find the smallest positive value of the original sample.
11:        $\mathbf{S}[i] \leftarrow s_i$ 
12:     end for
13:      $\mathbf{X}_{\text{fwd}} \leftarrow \text{where}(\mathbf{M}, \mathbf{S}, \mathbf{X})$  ▷ This is the desired output value.
14:     ▷ Step 2: Construct the final output to define the backward pass (STE)
15:      $\mathbf{X}_{\text{out}} \leftarrow \text{detach}(\mathbf{X}_{\text{fwd}}) + (\mathbf{X} - \text{detach}(\mathbf{X}))$  ▷ The following line implements STE using the detach trick.
16:     ▷ Forward pass uses the value of  $\mathbf{X}_{\text{fwd}}$ ; backward pass gradient flows through  $\mathbf{X}$ .
17:     return  $\mathbf{X}_{\text{out}}$ 
18: end procedure

```

A.6 SUPPLEMENTARY DETAILS AND RESULTS OF EXPERIMENTS

A.6.1 EXPERIMENT DETAILS

All experiments were conducted on the CIFAR-10 and CIFAR-100 datasets using their standard training and testing splits. For data augmentation during training, we applied random crops with a size of 32 pixels and a padding of 4 pixels and random horizontal flips, together with cutout. All input images were normalized by subtracting the dataset’s channel-wise mean and dividing by the standard deviation. For SNN-specific input, we used direct encoding, where the preprocessed static image is presented to the network at each of the $T = 4$ time steps. For our main performance

evaluation, we used VGG-16, VGG-19, and SEW-ResNet-18 (Fang et al., 2021a) as backbone architectures. In each model, we replaced the standard convolutional blocks (e.g., Conv-BN-ReLU) with our proposed E-I circuit. The classification head was simplified to a single linear layer that outputs logits. For the ablation studies and visualizations presented in the main paper, VGG-8 was used on the CIFAR-10 dataset. In all SNN models, the membrane time constant for excitatory neurons was set to $\tau_E = 2$.

All models were trained for 300 epochs with a batch size of 128. We used an SGD optimizer with a momentum of 0.9 and a weight decay of $5e-4$. The learning rate was managed with a cosine annealing schedule, which included a linear warmup from 0 to a peak learning rate of 0.01 for VGG-16/19 and ResNet-18 (0.02 for VGG-8/11) over the first 30 epochs for VGG-16/19 and ResNet-18 (10 epochs for VGG-8/11). The training objective was optimized using the standard cross-entropy loss function.

All experiments were implemented using the PyTorch framework and trained on NVIDIA RTX4090 GPUs.

A.6.2 EMPIRICAL ANALYSIS OF GRADIENT IMBALANCE

Figure 4 shows the magnitudes of gradient norms for all trainable parameters across all layers of a VGG-8 network in the first iteration. The mean gradient norm for the inhibitory synaptic weight, W_{EI} , in each layer is highlighted by a black arrow, revealing a significant imbalance compared to excitatory weights.

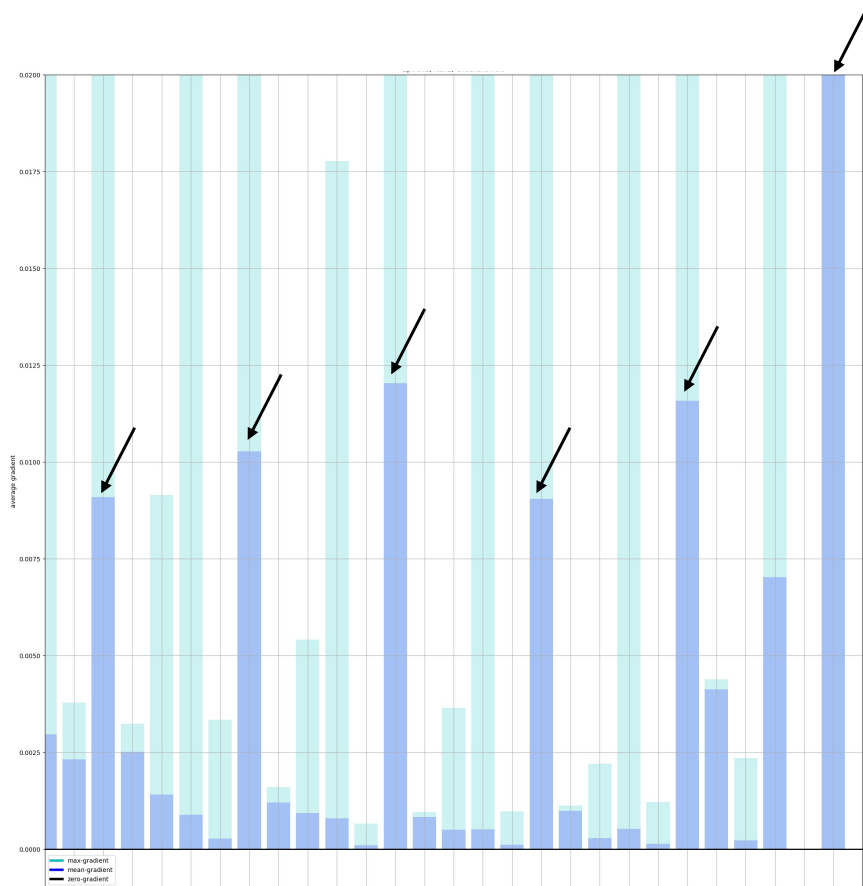


Figure 4: Empirical analysis of gradient norms at initialization.

A.6.3 COMPARISON BETWEEN OUR METHODS AND ANNS THAT ADHERE TO DALE’S LAW

The comparison with DANN (Cornford et al., 2021) highlights the advantages of our methods. Figure 5 shows that our model consistently outperforms DANN across all tested VGG architectures. Besides, the performance advantage of our methods widens as the network depth increases. The accuracy gap grows from a modest 0.57% on VGG-8 to a substantial 3.08% on VGG-19. This trend strongly suggests that our proposed mechanisms, E-I Init and E-I Prop, are particularly effective at preserving stable signal propagation and enabling effective learning in very deep architectures.

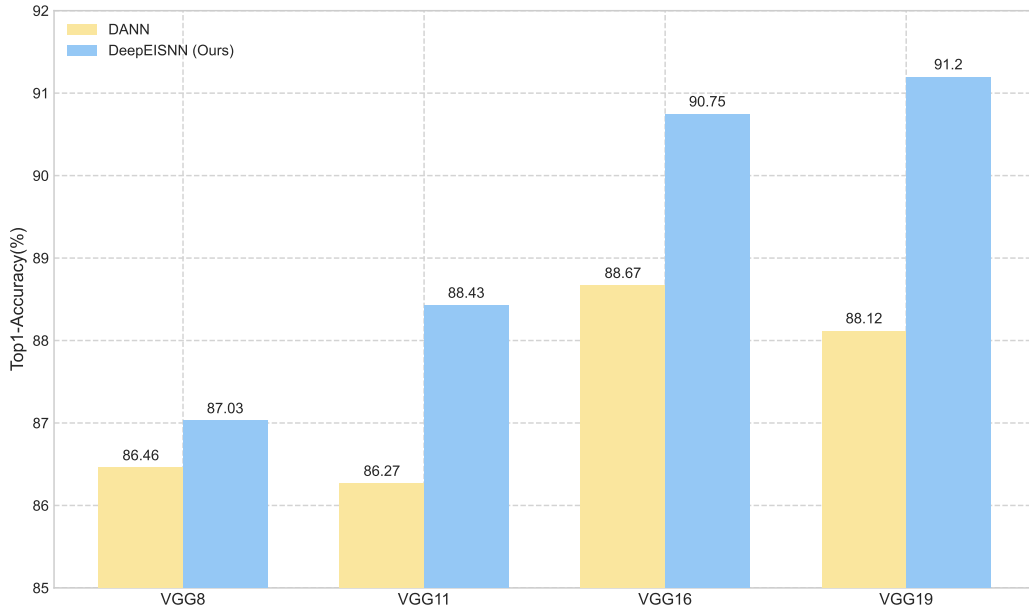


Figure 5: Comparison between our methods and DANN on CIFAR-10.

A.6.4 DISTRIBUTION OF BN OUTPUTS

Figure 6 demonstrates the distributions of the 1st, 3rd and 5th BN layer outputs after training in VGG-8.

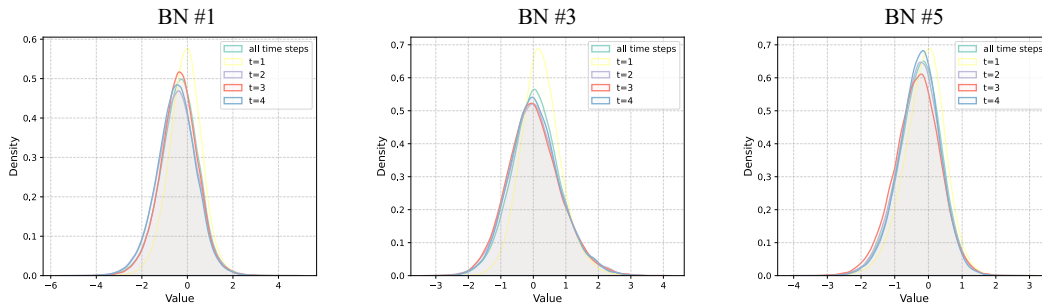


Figure 6: Distributions of the outputs in the 1st, 3rd and 5th BN layers after training.

A.6.5 VISUALIZATION OF E-I INTERACTIONS

A visual comparison of the feature maps suggests that our E-I circuit and a standard Batch Normalization (BN) layer focus on different aspects of the features. As shown in Figure 7, our E-I circuit

produces a sparse feature map where activations are concentrated along the object's contours, indicating a learned focus on feature edges and boundaries. In contrast, a standard BN layer would preserve the dense spatial output of its preceding convolution, normalizing the representation of the feature's overall shape and texture rather than isolating its boundaries. This suggests the two modules promote different computational strategies: the E-I circuit encourages a sparse, edge-centric representation, while BN supports a dense, holistic feature representation.

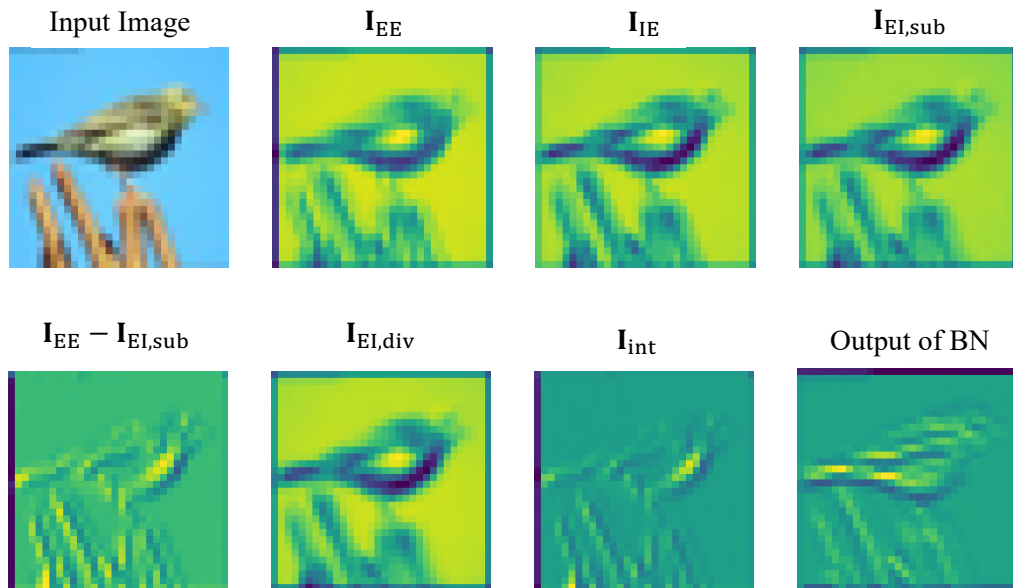


Figure 7: A comparison between feature maps of the first E-I circuit layer in our model and the feature map of the first BN layer in SNN with default BN after training.